PCCP

A direct simulation of EPR slow-motion spectra of spin labelled phospholipids in liquid crystalline bilayers based on a molecular dynamics simulation of the lipid dynamics

P. Håkansson,[a] P. O. Westlund,*[a] E. Lindahl[b] and O. Edholm[b]

[a] *Department of Chemistry, Biophysical Chemistry, Umeå University, SE-901 87 Umeå, Sweden*
[b] *Theoretical Physics, Royal Institute of Technology, KTH, SE-100 44 Stockholm, Sweden*

Received 26th June 2001, Accepted 5th September 2001
First published as an Advance Article on the web 13th November 2001

EPR line shapes can be calculated from the stochastic Liouville equation assuming a stochastic model for the reorientation of the spin probe. Here we use instead and for the first time a detailed molecular dynamics (MD) simulation to generate the stochastic input to the Langevin form of the Liouville equation. A 0.1 μs MD simulation at $T = 50\,^{\circ}C$ of a small lipid bilayer formed by 64 dipalmitoylphosphatidylcholine (DPPC) molecules at the water content of 23 water molecules per lipid was used. In addition, a 10 ns simulation of a 16 times larger system consisting of 32 DPPC molecules with a nitroxide spin moiety attached at the sixth position of the sn2 chain and 992 ordinary DPPC molecules, was used to investigate the extent of the perturbation caused by the spin probe. Order parameters, reorientational dynamics and the EPR FID curve were calculated for spin probe molecules and ordinary DPPC molecules. The timescale of the electron spin relaxation for a spin-moiety attached at the sixth carbon position of a DPPC lipid molecule is 11.9×10^7 rad s^{-1} and for an unperturbed DPPC molecule it is 3.5×10^7 rad s^{-1}.

1 Introduction

The spin labelling EPR technique has been successfully used for more than 20 years for studies of dynamics and structure of lipids in model membranes, in particular of the dipalmitoylphosphatidylcholine (DPPC)/water system.[1,2] Simulation of EPR spectra of spin labelled molecules has revealed a high sensitivity to molecular reorientation occurring at a timescale of 1–40 ns. This matches the correlation times for the reorientation of most lipid molecules but is slower than the internal hydrocarbon dynamics in liquid crystalline phospholipid bilayers. In systems with complex dynamics, the EPR spectra do not lend themselves to an easy immediate dynamical interpretation. A common procedure is then to assume a model for the dynamics and calculate the spectrum from that. If it does not match experiment one may vary parameters and models until a reasonable fit is obtained. Since the relation between the spectrum and the dynamics is quite complicated, the solution to this problem need not be unique and may also be difficult to find. The progress of simulation techniques and faster computers makes it now possible to simulate the detailed dynamics at an atomic scale of a small piece of lipid bilayer for timescales up to the order of 100 ns. If the atomic force parameters that are the basis for these simulations can be trusted, this gives us a tool to calculate spectra and to validate models for lipid dynamics. Conversely, the comparison between calculated and experimental spectra gives us another test of the atomic force parameters. Finally, there are definitely some differences between the dynamics of spin-labelled and non-labelled lipids. The question is whether these differences are important or not. Simulation provides a technique by which we may directly compare the dynamics of labelled and non-labelled lipids and even calculate the spectrum one would expect if the unpaired electron could be attached to the lipid without the perturbation of the clumsy spin probe. One may expect that a spin-probe PC lipid would reorient more slowly than a DPPC molecule because of the nitroxide moiety.

The main objective of this work is to illustrate the possibility of calculating slow-motion EPR spectra directly from trajectories of lipid reorientation obtained from MD simulations of a DPPC bilayer system. In this work, we need to specify what is meant by saying that a DPPC molecule with a nitroxide moiety attached at C_6 at the lipid acyl chain sn2, reorients in the same fashion as the lipid molecules forming the bilayer phase. In doing so we mimic a "spin-probe" molecule by defining an appropriate molecular fixed frame on the DPPC molecule. The principal frame (P) of the electron–lattice interactions of a nitroxide group attached for instance to carbon C_6 on sn2 is assumed to be collinear with the axis defined by carbon atoms C_5 and C_7. This "spin probe" molecule is denoted C_5C_7-DPPC. Similarly, a nitroxide spin moiety attached at C_{14} is assumed to reorient in the same fashion as $C_{13}C_{15}$-DPPC. Consequently, a real spin-labelled lipid molecule with the nitroxide spin moiety attached at C_n is reasonably approximated by the reorientation of an ordinary lipid molecule with the z-axis of the "principal frame" fixed at C_{n+1} and C_{n-1}. These "spin probe" molecules are also compared with a C_1C_{14}-DPPC molecule which should mimic more pronouncedly the overall lipid wobbling in the bilayer. Quantifying lipid reorientation motion in the MD simulation of DPPC has been done in ref. 3 where an inertia tensor of the whole lipid molecule is used to determine long axis reorientation. Looking at this whole molecule property instead of a principal system of a spin probe makes their reorientation analysis irrelevant in the context of the spectroscopic quantity which we are interested in. There are other reported MD simulation[4–6] but there is no analysis relevant and comparable with our EPR guided analysis.

We found from the 10 ns MD simulation, containing 32 spin-labelled 6PC molecules in a lipid matrix of 992 DPPC molecules, that the molecular reorientational correlation func-

DOI: 10.1039/b105618m

tion and order parameter of a real spin probe molecule 6PC is reasonably well described by C_5C_7-DPPC "spin probe". The reorientational correlation functions of 6PC and a C_5C_7-DPPC molecule were slightly different at short times. The EPR spectrum of 6-PC is slightly broader. This test indicates that we may identify EPR spectra of *n*PC with spectra obtain from C_{n+1} C_{n-1}-DPPC "spin probe" molecules from a MD simulation.

Almost all analysis of experimental EPR slow-motion lineshapes of lipid bilayer model systems is based on the stochastic Liouville equation (SLE) in the Fokker–Planck form. This is an approach developed about 25 years ago by Freed and coworkers.[2,7–9] The spectral simulations are cumbersome because they require explicit dynamic models of the lipid acyl chain segment and overall molecular reorientation in combination with the quantum mechanical spin model.[2,7–11] Simple diffusion models such as anisotropic rotational diffusion are combined with the quantum mechanical model. This is possible because for these simple models there exists an eigenfunction expansion of the rotation diffusion operator. The diffusion model defines parallel and perpendicular rotation diffusion coefficients ($D_\perp$, $D_\parallel$) which describe the lipid reorientation along and perpendicular to the molecular long axis. Moreover, an ordering potential must be introduced in order to describe the confined lipid motions in terms of order parameters, S_n. The potentials most often used are the familiar Maier–Saupe form $U(\cos\beta)/kT = -\lambda P_2(\cos\beta)$[2,7–9] or the simple cone potential.[12–14] Kothe *et al.*[10] also included a discrete *trans–gauche* conformation dynamics in order to compare EPR and ^{2}H NMR results within the same dynamics model. Characteristic order and dynamic parameters of phospholipids obtained from EPR studies are summarized in terms of S_0 and correlation times $\tau_\perp(=1/6D_\perp)$ and $\tau_\parallel(=1/6D_\parallel)$ or $\tau_R(=1/\sqrt{36D_\perp D_\parallel})$. The latter are found in the range 1–60 ns.[2,7–11] The order parameters S_0 of spin probes like 5PC or 6PC are found to be in the range 0.4–0.7.[1,2,7–11] Lipid reorientational diffusion in a potential certainly gives a simplified description of lipid dynamics in a bilayer. Still, all analysis of experimental work uses diffusion models and it seems as though they include the essential dynamics for EPR spectral simulations.

A MD simulation describes the lipid reorientation in a different language. The reorientational correlation function is calculated for different spin-labelled DPPC molecules. We found that initially there is a fast decay in the ps regime and a slow decaying tail, characterized by a correlation time of about 4 ns.[15] The alternative approach to SLE in the Fokker–Plank form discussed above is SLE in the Langevin form. The lipid dynamic model is then explicitly obtained from the MD or Brownian dynamics (BD) simulation model and incorporated into the SLE of the electron spin slow-motion formalism. The lipid molecular reorientation yields trajectories describing the fluctuation of a spin–lattice coupling Hamiltonian. This makes this approach more convenient when computer simulation models are available. Indeed, we have used the description of lipid dynamics from a 100 ns MD simulation to generate the fluctuating spin–lattice coupling Hamiltonian.

This is a relatively new approach. A few papers have previously dealt with direct calculation of EPR slow-motion spectra using Monte Carol (MC) or BD simulation techniques.[16–18] It was believed ten years ago that it was only possible to use BD for explicit dynamic models of complex molecular systems. At that time a synthesis of the slow-motion line shape theory with BD models was not available.[19] However, since then slow-motion EPR spectra have been calculated directly using BD-simulation models of lipid reorientation in a cone potential[20] and recently also including translational diffusion along curved (rippled) interfaces.[21] Using MD simulation a low number of independent trajectories are available since the lipid members are only 64–1024, whereas when MC or BD is used a sufficient number (10 000 or more) can easily be generated. Consequently, since few and relatively long electron spin density trajectories must be generated, a very accurate numerical algorithm is required. In Appendix A we present such an algorithm.[20]

In this paper a successful synthesis between the slow-motion line shape theory of EPR and MD simulation techniques is presented. Consequently, we demonstrate the possibility of using trajectories of lipid dynamics obtained from MD simulation in a direct calculation of slow-motion EPR line shapes.

The paper is organized as follows: First the slow-motion EPR line shape theory is reviewed. This theory is based on the stochastic Liouville equation in the Langevin form. The numerical algorithm developed to solve the SLE is presented in Appendix A. In the following section the molecular dynamics simulation model is presented. Direct simulation of EPR FID from MD trajectories is calculated. In the conclusions we sum up the main results which show that direct simulation of EPR slow-motion spectra using atomic simulations of the dynamics is feasible and gives a new way to validate MD simulation of lipid bilayers.

2 EPR slow-motion line shape calculations

2.1 The EPR line shapes function $I(\omega)$

The aim is to calculate the EPR line shape which is given as a Fourier–Laplace transform of the relevant spin density matrix element where the statistical average is explicitly given as an overbar. We do this because we want to clarify the Langevin form of SLE where we actually calculate the spin density matrix element (without overbar) for N (64, 1024) lipid molecules and then perform the statistical average:

$$\frac{dI(\omega)}{d\omega} = \mathrm{Re}\left\{-i\int_0^\infty t\, e^{-i\omega t}\,\overline{\rho_1^1(t)}dt\right\} \tag{1}$$

Here $\rho_1^1(t)$ is a time-dependent electron spin density matrix element containing the information on the magnetization in the xy-plane perpendicular to the applied magnetic field. In order to determine the time dependence of $\rho_1^1(t)$ we go to the Liouville equation:

$$\frac{d}{dt}\rho(t) = -iL\rho(t) = \frac{i}{\hbar}(\rho(t)H(t) - H(t)\rho(t)) \tag{2}$$

The coupling between the spin system and the rest of the system contain classical reorientational degrees of freedom which makes the Liouville operator explicitly time dependent. That is, it is given by the time dependence of the Hamiltonian, $H(t)$. The Liouville von Neumann equation becomes the stochastic Liouville equation by introducing the time dependence of the Hamiltonian through stochastic coefficients. Thus in order to describe slow-motion EPR spectra of a lipid bilayer we rely on the direct approach using the SLE in the Langevin form.[20,21] In the Langevin approach the explicit stochastic time-dependence of the spin Hamiltonian, SLE transform into a set of coupled stochastic differential equation

$$\frac{d}{dt}\rho(t) = -i[L_0^s + L_{SL}(t)]\rho(t), \tag{3}$$

where superoperators L_0^s and $L_{SL}(t)$ are defined through the respective Hamiltonian. The stochastic Liouville super operator $L_{SL}(t)$ has been constructed from the MD-trajectories of lipid reorientation of the DPPC/water system.

2.2 The spin Hamiltonian model

Consider the spin Hamiltonian of the spin-probe molecule (a nitroxide group attached to a PC-lipid) residing in a lipid

bilayer. The electron spin system with spin quantum number $S = 1/2$ is coupled to a nuclear spin system with spin quantum number $I = 1$. The time-independent Liouville spin operator L_0^S is then generated by the electron spin Hamiltonian: the Zeeman interaction $\omega_0 B_Z S_Z^1$ and the hyperfine interaction $AS_Z^1 I_Z^2$. B_Z is the static magnetic field of the spectrometer, ω_0 is the electron Larmor frequency and S_Z^1 is the z-component of a spherical irreducible spin tensor operator of rank 1 (thus a vector spin operator component $\boldsymbol{S}_z$). The time-dependent Liouvillian $L_{SL}(t)$ is generated by the anisotropic hyperfine interaction $H_{SL}^A(t)$ and the anisotropic part of the Zeeman interaction $H_{SL}^g(t)$. These two Hamiltonians are here written as a scalar product between irreducible spherical electron spin tensor operators and stochastic time-dependent lattice-tensor functions.[22]

$$H_{SL}^g(t) + H_{SL}^A(t) = \sum_{\alpha=g,\,A} \sum_n (-1)^n A_n^{2(L),\,\alpha} \sum_m F_{-k}^{2(P)\alpha} \overbrace{\times D_{km}^2[\Omega_{PD}(t)] D_{mn}^2[\Omega_{LD}]}^{\text{MD-simulation}} \quad (4)$$

where $A_n^{2(L)\alpha}$ is a second rank electron spin operator of interaction α taken in the laboratory fixed frame (L). Instead of the stochastic time-dependent tensor ($F_n^{2(L)}(t)$) of the lab-frame it is expressed in terms of the time-independent principal components $F_k^{2(P)}$ and stochastic time-dependent Wigner rotation matrix elements. The intermediate coordinate system (D) of the director frame of the lamellar phase describes the orientation with respect to the static magnetic field. The time modulation of the spin–lattice coupling $F_n^{2(L)}(t)$ is thus due to local anisotropic reorientational motion of the lipids in the bilayer. The transformations between coordinate systems are here illustrated by arrows as follows: Ω_{LD} is static and relates the lab-frame (L) $\rightarrow$ to the director frame (D); $\Omega_{DP}(t)$ relates the director frame (D) $\rightarrow$ to the (P)-frame. The Zeeman interaction tensor components of the principal frame (P) are given by

$$F_0^{2(P),\,g} = \sqrt{\frac{2}{3}} \left(\frac{\beta_e}{\hbar}\right)[g_{zz} - \tfrac{1}{2}(g_{xx} + g_{yy})]; \quad F_{\pm 1}^{2(P),\,g} = 0;$$
$$F_{\pm 2}^{2(P),\,g} = \frac{1}{2}\left(\frac{\beta_e}{\hbar}\right)(g_{xx} - g_{yy}) \quad (5)$$

where g_{xx}, g_{yy} and g_{zz} are the tensor diagonals in the principal frame and β_e is the Bohr magneton. The corresponding second rank spin operators taken in the lab frame are defined as

$$A_0^{2(L),\,g} = \sqrt{\tfrac{2}{3}}\, B_Z S_Z; \quad A_{\pm 1}^{2(L),\,g} = \mp \tfrac{1}{2} B_Z S_{\pm 1}; \quad A_{\pm 2}^{2(L),\,g} = 0. \quad (6)$$

The hyperfine interaction is given by the following lattice tensor components of the principal frame (P)

$$F_0^{2(P),\,A} = \sqrt{\frac{2}{3}} \left(\frac{g_e \beta_e}{\hbar}\right)[A_{zz} - \tfrac{1}{2}(A_{xx} + A_{yy})]; \quad F_{\pm 1}^{2(P),\,A} = 0;$$
$$F_{\pm 2}^{2(P),\,A} = \frac{1}{2}\left(\frac{g_e \beta_e}{\hbar}\right)(A_{xx} - A_{yy}) \quad (7)$$

where A_{xx}, A_{yy} and A_{zz} are the diagonal tensor elements in the principal frame and g_e is the trace of the g-tensor (see Table 1). The corresponding second rank spin operator taken in the lab frame is defined as

$$A_0^{2(L),\,A} = \sqrt{\tfrac{2}{3}}[S_Z I_Z + \tfrac{1}{4}(S_{+1} I_{-1} + S_{-1} I_{+1})];$$
$$A_{\pm 1}^{2(L),\,A} = \mp \tfrac{1}{2}(S_Z I_{\pm 1} + I_Z S_{\pm 1});$$
$$A_{\pm 2}^{2(L),\,A} = \tfrac{1}{2} S_{\pm 1} I_{\pm 1}. \quad (8)$$

The macroscopic orientation of the sample, expressed by the director frame of the lamellar phase, is chosen collinear with the B_0 field in the laboratory frame. The angle between the director z-axis (normal to the macroscopic lamellar sample, and the static magnetic field is $\beta_{LD} = 0°$. This orientation is chosen in order to get the increased sensitivity of anisotropic motion, as compared to the $\beta_{LD} = 90°$ orientation.[7] The Hamiltonian simplifies by assuming a cylindric symmetric tensor in the principal frame;

$$H_{SL}^g(t) + H_{SL}^A(t) = \sum_{\alpha=g,\,A} \sum_n (-1)^n A_n^{2(L),\alpha} \sum_m F_0^{2(P)\alpha} \overbrace{D_{0m}^2[\alpha_{PD}(t),\, \beta_{PD}(t)] D_{mn}^2[\Omega_{LD}]}^{\text{MD-simulation}}. \quad (9)$$

With this spin Hamiltonian the local motion present in the Euler angles is obtained from the MD simulation of the DPPC bilayer.

A complete set of spin operators is introduced which transforms the stochastic Liouville equation into a set of coupled stochastic differential equations of dimension nine.[20]

$$\frac{d}{dt}\rho(t) = -i[\boldsymbol{L}_0^S + \boldsymbol{L}_{SL}(t)]\rho(t). \quad (10)$$

This system of coupled stochastic equations is solved using the decomposition of the Liouville matrix into a sum of matrices with special symmetry properties. Then we applied the symmetrized Trotter's formula which is a very accurate numerical algorithm most convenient for long trajectories since it preserves the norm at every time step.[20] The algorithm is presented in more detail in Appendix A.

Table 1 Magnetic parameters used in EPR calculation, Hyperfine $\boldsymbol{A}$ and $\boldsymbol{g}$ tensors, magnetic field B_z and inhomogeneous line with T_2^{-1}

A tensor/G	g tensor	B_z	T_2^{-1}/G
$A_{xx} = 6.1$	$g_{xx} = 2.0088$	3200	1.0
$A_{yy} = 6.1$	$g_{yy} = 2.0088$		
$A_{zz} = 32.6$	$g_{zz} = 2.0027$		

3 The molecular dynamics computer simulations

3.1 Forcefield

The present MD simulations build on a force field for lipids originating from Berendsen's group.[5,23] The parameters for the hydrocarbon part were reparametrized by using data for liquid pentadecane by Berger *et al.*[24] This also gave improved agreement for experimental volumes and areas per lipid. It has later been used in extensive simulations[15,25,26] in which a number of properties of lipid liquid crystalline DPPC bilayers are in favourable agreement with experiment. The simulations presented here use the forcefield of system II from ref. 24, but with slightly smaller charge groups (atoms 1–4, 5–7, 8–11, 12–14, 15–16 and 32–35).

The spin-labeled lipids were modeled by attaching a five atom ring to the appropriate carbon atom in the DPPC chain, and replacing the CH_2 united atom parameters with C parameters. The bonded interactions in the spin probe were taken from the Gromos87 force field, resulting in an N–O bond in the nitroxide spin probe that was oriented parallel to the local chain direction at the position where the spin probe was attached. The hydrocarbon groups in the ring were treated as united atoms. Since the surrounding nonpolar hydrocarbon chains were modeled without charges and no external field was applied we assumed that the main influence on the chain motion from the spin probe is due to the weight and steric hindrance. By adding charges to the spin probe, the amount of interaction of the spin probe with the environment will increase and make the motion even slower, but to make sure these were not overestimated we chose to perform the full simulation without charges on the spin probe.

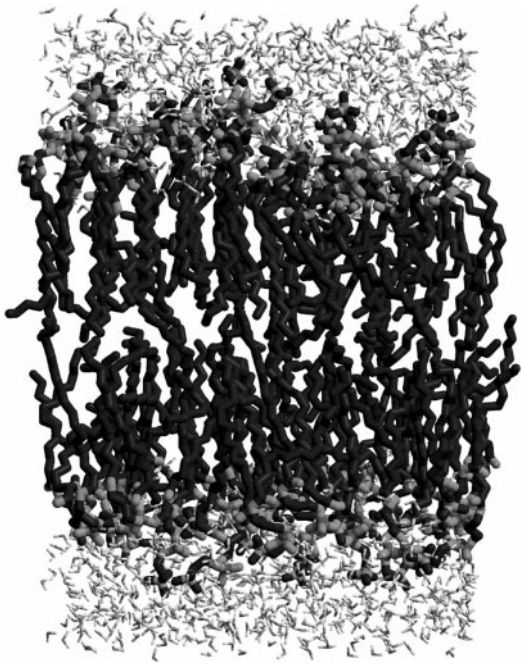

Fig. 1 The system after 100 ns simulation. Water is drawn as thin rods, lipids as thicker. Carbon atoms are dark and other lipid atoms lighter. The roughness of the interface and deeply buried waters are clearly visible.

3.2 Set-up

A system was prepared by randomly placing 64 lipids from an earlier simulation in two layers with 3 nm separation. Each lipid was randomly rotated and tilted up to 30°. The z coordinates, determined from the position of the carbon connecting the two chains in each lipid, were given a spread of ± 0.3 nm in each layer. This structure was relaxed with 500 steps of energy minimization, after which 23 SPC waters per lipid were added outside a hydrocarbon core of 3.2 nm thickness. This structure was finally subjected to 1000 energy minimization steps.

To relax fluctuations from regions of high pressure the system was run for 50 ps at constant volume, scaling the temperature of lipids and water separately to heat baths[27] at 323 K with a time constant of 0.05 ps. This was followed by another 50 ps run with identical temperature scaling in combination with pressure scaling to 1 atm in all directions with a constant of 0.5 ps. Both time constants were then doubled, and the system simulated for another 100 ns. Fig. 1 displays a snapshot of the bilayer system simulated, the end frame is after 100 ns.

All runs were performed with the GROMACS molecular dynamics package.[28] A time step of 2 fs was used while all bond lengths were kept constant using the LINCS algorithm.[29] A cut-off at 1.0 nm was used for the Lennard-Jones interactions and 1.8 nm for electrostatics, the long-range coulomb forces being updated every 10 steps. 1,4 electrostatic interactions were reduced by a factor of 2 and 1,4 Lennard-Jones interactions by a factor of 8. Bond rotations in the carbon tails were modelled with Ryckaert–Belleman[30] dihedrals and the corresponding 1,4 interactions removed.

4 Results and discussions

Here we first give some general results about the lipid organization and dynamics of the DPPC molecules. Then, we turn to the analysis of the MD simulation with respect to what is relevant for EPR spectral analysis. Consequently, when we talk about "reorientation of DPPC molecule" it refers to the reorientation of a frame with its z-axis defined by two carbon atoms on the acyl chain. Six "spin-probe" DPPC molecules are studied namely; C_5C_7-DPPC, C_6C_7-DPPC, $C_{13}C_{15}$-DPPC, $C_{14}C_{15}$-DPPC, C_1C_{16}-DPPC and 6PC. In the simulation with 6PC the orientation of the principal frame is oriented with the z-axis orthogonal to the C–N–C bond of the spin probe.

For these spin-probe molecules the time modulation of the spin–lattice coupling is determined by the MD simulation (*cf.* eqn. (9)). This modulation causes spin relaxation and line broadening. Stochastic data were extracted both from a 100 ns MD simulation of 64 DPPC molecules and a 10 ns MD simulation with 32 6PC spin probe molecules inserted into the equilibrated bilayer of 992 DPPC molecules. The coordinates of the molecular frames at sn1 and sn2 were stored every picosecond. To study short-time molecular relaxations, data was also stored 10 times denser during the first 10 ns of the run.

4.1 Static properties

Fig. 2 shows the variations in area and volume per lipid together with the bilayer repeat distance during the simulation. The volume is clearly the most stable of these. With an average of 1.219 nm^3 it deviates less than 1% from the experimental result 1.232 ± 0.012 nm^3.[31] Both the area and the bilayer repeat distance show large fluctuations, which are anti-correlated since the volume is roughly constant. Interestingly, the system exhibits important dynamics and oscillations on timescales in the order of 10 ns despite the small size of the system. The average area per lipid during the simulation is 0.61 nm^2, but with quite a large spread of 0.02 nm^2. This is smaller than the experimental area, but by simulating larger systems we have determined this to be a finite system size effect.[25] The area dependence on the number of lipids N in the system is well described by the relation $A(N) = (0.634–1.28/N)$ nm^2, which for an infinite system is in agreement with the experimental[32] 0.629 ± 0.013 nm^2. These results also suggest that it might be questionable whether one can determine an accurate equilibrium area per lipid from simulations shorter than tens of nanoseconds for systems with hundreds of lipids.

The snapshot of the simulated system at the end frame of 100 ns (Fig. 1) shows a substantial spread in the z-distribution of lipids due both to random protrusions and collective undulations, the latter is also possibly responsible for the long-time dynamics. By spectral analysis[25] the RMS amplitude of the undulations was determined to be 0.1 nm, and the total

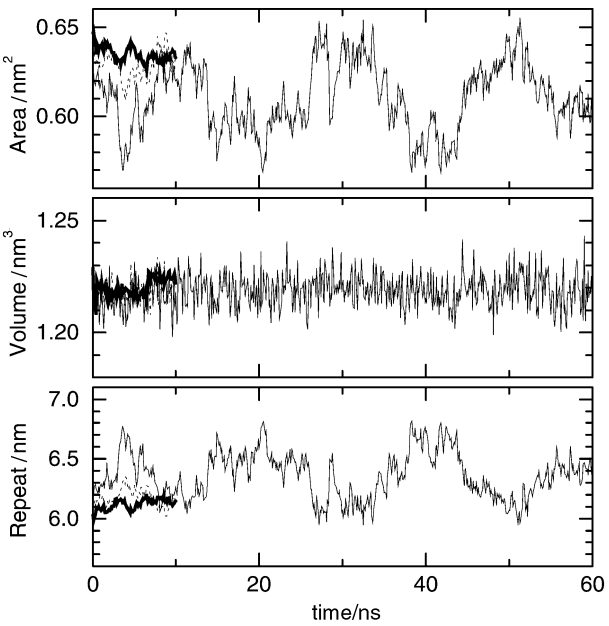

Fig. 2 Time development of area and volume per lipid and bilayer repeat distance during the simulation. Although the volume is fairly constant, both area and repeat show large oscillations on scales up to 10 ns.

average lipid RMS z-displacement to be 0.24 nm. The solvent waters penetrate through the head-group region but not into the hydrophobic core.

4.1.1 Spin-probe order parameters. Spin-probe order parameters are defined by the average of the Wigner rotation matrix element; $S_n = \langle D^2_{n0}[\Omega_{PD}]\rangle^2$ where the Euler angles $\Omega_{PD} = (\alpha_{PD}, \beta_{PD})$ define the orientation of the molecular fixed z-axis C_{k-1}–C_{k+1} relative to the director frame. S_n with $n \neq 0$ were approximately zero, as expected for a three-fold or more rotation symmetry around the z_D axis. The order parameter S_0 is given in Table 2 for different "spin-probe" DPPC-molecules. S_0 for C_5C_7-DPPC and $C_{13}C_{15}$-DPPC can be compared with those for C_6C_7-DPPC and $C_{14}C_{15}$-DPPC respectively. As expected, the order parameters of C_nC_{n+1}-DPPC molecules are considerably smaller than the values obtained from experimental studies. The largest order parameter, $S_0 = 0.65$, is obtained for the C_1C_{16}-DPPC molecule. It corresponds to the order parameter of the molecular long axis, a wobbling potential. The order parameters of the sn2 chain are similar to the sn1 order parameters except at the end of the chain ($C_{14}C_{15}$-DPPC where sn2 is clearly stiffer with $S_0 = 0.178$ compared to $S_0 = 0.042$ for sn1). In Table 3 the three order parameters: the 6PC spin probe ($S_0 = 0.344$), the DPPC-lipid molecules in the same lipid matrix as the spin-probe molecule (denoted with *) and the unperturbed DPPC molecules have been calculated from a 10 ns MD simulation of 1024 DPPC molecules forming the bilayer. The order parameter of 6PC is smaller than that of the DPPC molecules without the nitroxide moiety. Notice also that 6PC seems not to perturb the order of the rest of the DPPC molecules forming the bilayer.

4.2 The reorientation of "spin-labeled" DPPC

Fig. 3 shows the reorientational correlation functions $g(t)$ defined by the second Legendre polynomials

$$g(t) = \langle P_2(\cos(\theta(t) - \theta(t_0)))\rangle \equiv \sum_n \langle D^{2*}_{n0}[\Omega_{PD}(t)] D^2_{n0}[\Omega_{PD}(t_0)]\rangle, \quad (11)$$

averaged over different t_0. There is a considerable drop from fast motions during the first few picoseconds, but the main relaxation occurs on a scale of approximately 1 ps up to 10 ns. As anticipated, the relaxation is faster closer to the end of the chains and the limiting value at large times is much lower, corresponding to the more disordered state of the chains (it is directly related to the order parameter). The relaxation for the C_5C_7-DPPC vectors has two distinct regions, with a turnover around 10 ps. The $C_{13}C_{15}$-DPPC vectors, in contrast, show a more continuous decay throughout the plot, but also in this case two regions are present, only less pronounced.

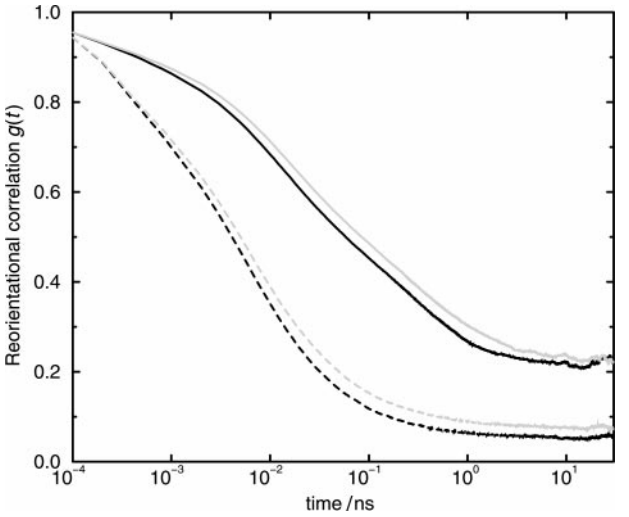

Fig. 3 The reorientational correlation function P_2 of carbon chain vectors. Solid lines represent the C_5–C_7 vectors, while the C_{13}–C_{15} are dashed. sn1 relaxations are drawn black while the sn2 ones are grey.

The decay is much more stretched than can be described with a single exponential relaxation time. One way to represent this kind of dynamics is with so-called stretched exponential functions:

$$g(t) = e^{-(t/\tau)^\beta} \quad (12)$$

By plotting $\ln(-\ln(g(t)))$ *vs.* logarithmic time in the inset graph the exponent β is obtained as the slope. From this we determined the dynamics of C_5C_7-DPPC of sn1 to be best

Table 2 Ensemble averages for carbon vectors representing "spin-probes" on sn1 and sn2 carbon chains in a 64 lipid matrix. $S_0 = \langle D^2_{00}[\Omega_{DP}]\rangle$ is the order parameter, where Ω_{DP} are Euler angles of the molecular fixed z-axis relative to the director frame. Order parameters $S_n = \langle D^2_{n0}[\Omega_{DP}]\rangle$ with $n \neq 0$ are approximatively zero

	S_0	$\langle \lvert D^2_{00}[\Omega_{DP}]\rvert^2\rangle$	$\langle \lvert D^2_{10}[\Omega_{DP}]\rvert^2\rangle$	$\langle \lvert D^2_{20}[\Omega_{DP}]\rvert^2\rangle$
sn1				
C_1C_{16}-DPPC	0.62	0.50	0.206	0.043
C_5C_7-DPPC	0.470	0.398	0.224	0.076
C_6C_7-DPPC	0.072	0.176	0.240	0.172
$C_{13}C_{15}$-DPPC	0.232	0.279	0.224	0.136
$C_{14}C_{15}$-DPPC	0.042	0.197	0.216	0.185
sn2				
C_1C_{16}-DPPC	0.65	0.521	0.202	0.375
C_5C_7-DPPC	0.481	0.404	0.224	0.074
C_6C_7-DPPC	0.332	0.323	0.229	0.110
$C_{13}C_{15}$-DPPC	0.274	0.302	0.224	0.125
$C_{14}C_{15}$-DPPC	0.178	0.266	0.215	0.152

Table 3 Order parameter and mean square values of the MD-simulation of the 6PC molecule (sn2 chain), the $C_5C_7^*$-DPPC labelled molecule in the lipid matrix, slightly perturbed by the 6PC molecule, and the C_5C_7-DPPC labelled molecules in the pure lipid matrix (sn2 chain). Averages were calculated from a 10 ns MD-simulation of 32 6PC trajectories, 992 $C_5C_7^*$-DPPC trajectories and 1024 C_5C_7-DPPC trajectories. The error in S_0 is estimated from student-t distribution ($\pm t_{0.95,N}\sqrt{(\sigma^2_N/N)}$) using all vectors ($N \sim 10^4$) in one trajectory as one batch

	S_0	$\langle \lvert D^2_{00}[\Omega_{DP}]\rvert^2\rangle$	$\langle \lvert D^2_{10}[\Omega_{DP}]\rvert^2\rangle$	$\langle \lvert D^2_{20}[\Omega_{DP}]\rvert^2\rangle$
sn2				
6PC	0.344 ± 0.05	0.32	0.23	0.11
$C_5C_7^*$-DPPC	0.425 ± 0.006	0.374	0.226	0.09
C_5C_7-DPPC	0.427 ± 0.006	0.376	0.225	0.09

described by two stretched exponents in different regions, using $\beta = 0.5$ and $\tau = 37$ ps on scales shorter than approximately 20 ps (dot-dashed line), and $\beta = 0.36$, $\tau = 63$ ps for slower relaxations (dashed line). Due to the exponent, τ is not directly related to the usual exponential relaxation time. The origin of the stretched decay is the complicated dynamics in the system which cannot be characterized by a single decay rate. One way to understand the results is to assume a distribution of free energy barriers for the orientational dynamics responsible for the correlation function, the *trans–gauche* isomerization in the hydrocarbon tails. Such an isomerization around a bond in a free chain is characterized by a single barrier. However, the isomerization around one bond affects the reorientation of other segments in the chain and the ordering of other chains through steric repulsion, introducing correlations. These processes give rise to a broad distribution of free energy barriers. From this we can deduce a relaxation (assuming the transition rate for each barrier height to be proportional to $\exp(-E/k_BT)$, see ref. 33) which is

$$g(t) = \int \mathrm{d}E\rho(E)\exp(-r_0\, te^{-E/k_BT}) \qquad (13)$$

were $\rho(E)$ is the barrier height distribution. Assuming a Gaussian distribution of barriers we can calculate the relaxation and get an acceptable fit (solid curve in Fig. 4) for a Gaussian of width 2.5 in units of k_BT. It is also possible to invert (*cf.* eqn. (13)), which for a stretched exponential $g(t)$ yields a half width of the barrier height distribution approximately equal to the inverse exponent β.

4.3 Electron spin relaxation in DPPC-bilayer

In this section we present the direct calculations of the electron spin correlation function of the "spin probe" C_5C_7-DPPC molecule. Only the DPPC molecules with the "spin probe" attached on the sn2 chain is presented. The stochastic time-dependent Euler angles describing the lipid reorientation are obtained from MD-simulation and are introduced into the second rank tensor function of the spin–lattice Hamiltonian (*cf.* eqn (9)). Trajectories of the stochastic electron spin density matrix element $\rho_1^1(t)$ are generated using the algorithm of Appendix A and the 100 ns MD simulation. Since the MD simulation is in the fast motion regime, $\sqrt{\langle H_{SL}(t)H_{SL}(0)\rangle}\,\tau_c \ll 1$, a Red-field approximation[33] may also be used to estimate the EPR relaxation rate. The spin–spin relaxation rate is given by the Redfield relaxation matrix element

$$\hat{\mathscr{R}}_{\frac{1}{2}-\frac{1}{2}\frac{1}{2}-\frac{1}{2}} = J_0(0) + J_{-1}(\omega_0) \qquad (14)$$

where ω_0 is the Larmor frequency. The Redfield matrix element is expressed in the electron spin Zeeman basis. The spectral densities $J_0(0)$ and $J_{-1}(\omega_0)$ are given by the Fourier–Laplace transform of the time correlation function of the spin–lattice coupling,

$$J_n(\omega) = \int_0^\infty \mathrm{tr}_{IL}\{(T_n^1(t))^\dagger T_n^1(0)\sigma_{IL}\}\exp(-\mathrm{i}\omega t)\mathrm{d}t \qquad (15)$$

where the trace (tr) is taken over all nuclear spin and lattice degrees of freedom. The first rank tensor elements $T_n^1(t)$ include nuclear spin operators and the second rank the Wigner rotation matrix elements obtained from the MD simulation. The spectral densities of (*cf.* eqn (15)) were calculated numerically. The electron spin relaxation rates of the central line of the EPR spectra were estimated as $\mathrm{Re}\{\hat{\mathscr{R}}_{\frac{1}{2}-\frac{1}{2}\frac{1}{2}-\frac{1}{2}}\} = 3.5 10^7$ rad s^{-1} for C_5C_7-DPPC and $11.9 10^7$ rad s^{-1} for 6PC. In Fig. 5 the spin–spin electron correlation functions (FID), $\rho_1^1(t)$, are displayed together with the electron spin relaxation rate estimated from the Redfield theory. Notice that the electron spin relaxation process has not decayed on the timescale of our 100 ns MD-simulation. The electron spin FID was calculated directly from the 100 ns MD simulation of 64 lipid molecules (solid line). Because of the relatively slow electron spin relaxation process which is not completely relaxed within the rather long MD simulation interval it was not possible to obtain the EPR line shape by Fourier transforming this truncated FID. In order to calculate the EPR line shape and to get an illustrative example of our approach we have extrapolated the MD-FID using a flexible BD model. The result is displayed in Fig. 6 where the solid line represents the MD-FID and the dotted line the extrapolated FID. Clearly these line shapes, both for the spin C_5C_7-DPPC and the probe 6PC are narrow spectra and the MD-dynamics are fast enough for motional narrowing to apply. The extrapolation procedure used is possible since the reorientation correlation function of the spin–lattice coupling has relaxed on the timescale of the MD simulation. A flexible BD model which reproduces the lipid reorientation correlation function and does not add anything else subtle may thus be used to improve the statistical aspects in the direct calculation of the EPR spectrum. Consequently, we may also illustrate the effects of lipid reorientation

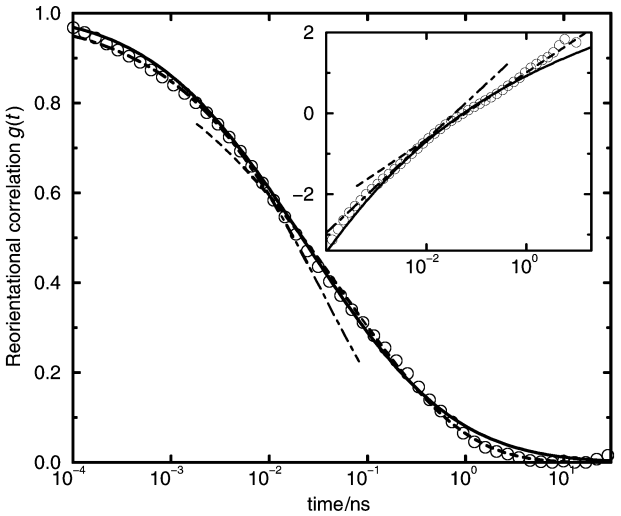

Fig. 4 Normalised time correlation function of the C_5–C_7 vector of sn1 chain (circles) together with fitted functions. The dot-dashed line is a stretched exponential with $\beta = 0.5$, $\tau = 37$ ps and the dashed one with $\beta = 0.36$, $\tau = 63$ ps. The solid curve is the relaxation calculated from a Gaussian barrier distribution of width 2.5 k_BT. The inset shows the same curves, but with $\ln(-\ln(g(t)))$ on the y-axis.

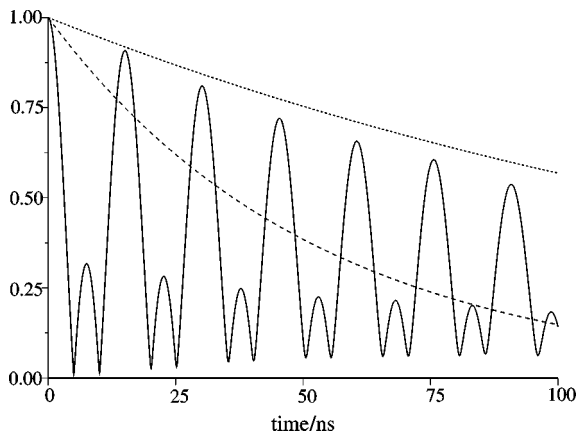

Fig. 5 The normalised electron spin–spin correlation function (FID) $\mathrm{Re}[\rho_{\pm1}^1(t)]$ is displayed for the C_5C_7-DPPC molecule directly calculated from the 100 ns MD simulation (solid line). The dotted line show the Redfield decay constant of the middle EPR-line whereas the semi-dotted line displays the same Redfield decay constant calculated for the real 6PC spin-probe molecule where the orientation correlation functions were numerically determined from the 10 ns MD-simulation.

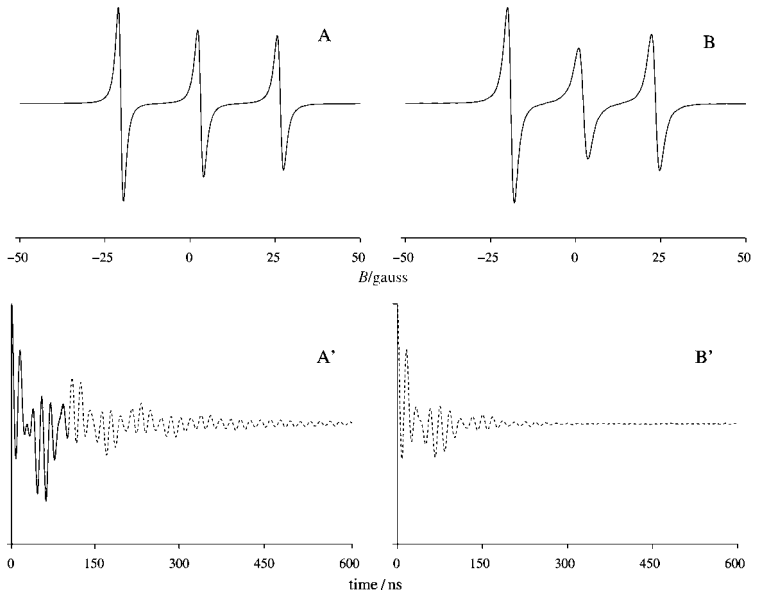

Fig. 6 The EPR line shapes of C_5C_7-DPPC (A) and 6PC spin probes (B) are displayed using extrapolated FID signals. The extrapolation is done by fitting the orientational correlation function of the MD simulation to a flexible BD model. Then the FID could be extended to longer times using the BD simulation. Notice in A′ and B′ the extended FID signals for the two spin probes. The solid line in A′ represents the FID calculated from the 100 ns MD simulation. The dotted line shows the extended FID. The Redfield decay constant was calculated for the extrapolated FID signals. We obtained A: (C_5C_7-DPPC) 4×10^7 rad s^{-1} and for B: (6-PC) 14×10^7 rad s^{-1} (which should be compared with the corresponding decay constants 3.5×10^7 rad s^{-1} and 11.9×10^7 rad s^{-1} obtained from the MD simulation).

in terms of EPR line shapes. This procedure has also been used in the simulation of EPR spectra in side chains in proteins.[35]

5 Conclusions

The direct calculation method based on the stochastic Liouville equation in the Langevin form has been used to calculate EPR slow-motion spectra using trajectories from a 100 ns MD simulation of a bilayer membrane model system. The reorientation of the DPPC molecules in the MD simulation was relatively fast and not in the so-called slow-motion regime since a substantial part of the decay occurs on sub-nanosecond timescales.

From a 10 ns simulation of a DPPC bilayer with 3 mol.% 6PC spin labels it was shown that the dynamics of spin-labelled lipids deviates from that of the C_5C_7-DPPC molecules. The EPR line shape of the former is slightly broader. Since we did not include the charges on the spin probe the effect we observe on the lipid chain motions can be regarded as a lower estimate, increased charges might lead to even slower dynamics. We believe that it is justified to compare the spin-probe dynamics with the reorientation of DPPC molecules with an appropriate defined molecular fixed "principal" frame. We found that neither of the two EPR spectra were typically slow-motion spectra. However, future MD studies may show that the spin-probe dynamics will fall into the slow-motion regime.

With this approach we have demonstrated an important connection between MD-simulation models of lipid model systems and spin-labelled EPR spectroscopy applied on real lipid membrane model systems. In previous BD simulations of EPR slow-motion spectra[20] it was shown that trajectories of about 2000 time points covering the time interval of the decayed FID gave a smooth spectrum. In order to obtain the best calculation possible the stationarity of the process is used when calculating the spin–spin electron correlation function. The average $\rho_1^1(t) = \langle S_1^1(t_0)S_1^1(t_0 + t)\rangle$ is calculated over different t_0. In the BD simulation where the complete decay of the FID is covered we obtain no real change in FID when the number of trajectories is increased to 1000, so 50 trajectories is sufficient. The algorithm is thus very suitable for MD simulation work and direct calculation of EPR/NMR spectra.

Acknowledgements

This work was supported with computing resources for Planning and Coordination of Research (FRN), Parallelldatorcentrum (PDC), Royal Institute of Technology and the Swedish Natural Science Research Council.

Appendix A. The algorithm solving the stochastic Liouville equation

The density operator is transformed to the interaction picture by

$$\boldsymbol{\rho}^*(t) = e^{i\boldsymbol{L}_0 t}\boldsymbol{\rho}(t) \tag{A.1}$$

thus eliminating the Zeeman resonance frequency (ω_Z). In the electron/nuclear spin system the differential equation for the density operator now reads

$$\frac{d\boldsymbol{\rho}^*(t)}{dt} = -i[\boldsymbol{L}_0^J{}^* + \boldsymbol{L}_A^*(t) + \boldsymbol{L}_g^*(t)]\boldsymbol{\rho}^*(t). \tag{A.2}$$

A formal solution of (*cf.* eqn. (A.2)) may be written as

$$\boldsymbol{\rho}^*(t - t_0) = \exp\left(-e^i \int_{t_0}^{t} \boldsymbol{L}^*(s)ds\right)\boldsymbol{\rho}^*(t_0) \tag{A.3}$$

where $\boldsymbol{L}^*(s) \equiv \boldsymbol{L}_0^J{}^*(s) + \boldsymbol{L}_A^*(s) + \boldsymbol{L}_g^*(s)$. The numerical counterpart of eqn. (A.3) used in this work is obtained using discrete times as $\tau = t_{j+1} - t_j$, giving the solution at each time step

$$\boldsymbol{\rho}^*(t_{j+1}) = e^{-ir\boldsymbol{L}^*(t_j)}\boldsymbol{\rho}^*(t_j). \tag{A.4}$$

At every time step the stochastic matrix $\boldsymbol{L}^*(t_j)$ is decomposed into a finite sum of matrices $\boldsymbol{L}^*(t_j) = \Sigma_{k=1}^{p} \boldsymbol{A}_k(t_j)$ with a special symmetry property. These matrices have all power ($n > 3$) expressed in terms of lower power as

$$\boldsymbol{A}_k^{2n}(t_j) = |f(t_j)|^{2n}\alpha_k^{2n-1}\boldsymbol{K}_k^2 \tag{A.5}$$

$$\boldsymbol{A}_k^{2n-1}(t_j) = |f(t_j)|^{2n-1}\alpha_k^{2n}\boldsymbol{K}_k \tag{A.6}$$

when $|f(t_j)|$ is a hyperfine tensor component (see eqn. (A.18)), α_k is a scalar and $\boldsymbol{K}_k$ is a matrix. With $\boldsymbol{L}^*(t_j)$ decomposed in

this way a symmetrized version of Trotter's formula may be applied

$$\exp\left(\sum_{k=1}^{p} \boldsymbol{A}_k\right) \approx e^{\boldsymbol{A}_1/2} \ldots e^{\boldsymbol{A}_{p-1}/2} e^{\boldsymbol{A}_p} e^{\boldsymbol{A}_{p-1}/2} \ldots e^{\boldsymbol{A}_1/2}. \quad \text{(A.7)}$$

The propagator of eqn. (A.4) is expressed using eqn. (A.7) as

$$e^{-i\tau \boldsymbol{L}^*(t_j)} = \exp\left[-ic_k \sum_{k=1}^{p} \boldsymbol{A}_k(t_j)\right]$$

$$\approx \boldsymbol{\Lambda}_1(t_j) \ldots \boldsymbol{\Lambda}_{p-1}(t_j) \boldsymbol{\Lambda}_p(t_j) \boldsymbol{\Lambda}_{p-1}(t_j) \ldots \boldsymbol{\Lambda}_1(t_j). \quad \text{(A.8)}$$

Each matrix of eqn. (A.8) is defined, using the symmetry properties of eqn. (A.5) and eqn. (A.6) as

$$\boldsymbol{\Lambda}_k(t_j) \equiv \boldsymbol{I} - i \sin(c_k |f(t_j)| \sqrt{\alpha_k}) \frac{\boldsymbol{K}_k}{\sqrt{\alpha_k}}$$

$$+ [\cos(c_k |f(t_j)| \sqrt{\alpha_k}) - 1] \frac{\boldsymbol{K}_k^2}{\alpha_k} \quad \text{(A.9)}$$

where the constant $c_k = \tau/2$ ($k = 1, \ldots, p-1$) and $c_p = \tau$. The Liouville superoperator of eqn. (A.2) is formulated in the complete set of operators

$$\{|\tfrac{1}{2}\rangle\langle -\tfrac{1}{2}| \otimes (|1\rangle\langle 1|, |0\rangle\langle 0|, |-1\rangle\langle -1|, |1\rangle\langle 0|, |0\rangle$$

$$\langle -1|, |0\rangle\langle 1|, |-1\rangle\langle 0|, |1\rangle\langle -1|, |-1\rangle\langle 1|)\} \quad \text{(A.10)}$$

From the complete 36 × 36, a submatrix of dimension 9 × 9 was chosen by fixing the magnetic electronspin quantum numbers as: $m_s = \frac{1}{2}$, $m_s' = -\frac{1}{2}$. A matrix element in the matrices below, suppressing the spin quantum number when writing, is: $(|\tfrac{1}{2}\rangle\langle -\tfrac{1}{2}| \otimes |m_I''\rangle\langle m_I'''|)\dagger A_k |\tfrac{1}{2}\rangle\langle -\tfrac{1}{2}| \otimes |m_I\rangle\langle m_I'|$, where the order of nuclear spin operators in the matrices is given in eqn. (A.10).

$$\boldsymbol{A}_1 \equiv \begin{pmatrix} 0 & 0 & 0 & 0 & 0 & 0 & 0 & 0 & 0 \\ 0 & 0 & 0 & 0 & 0 & 0 & 0 & 0 & 0 \\ 0 & 0 & 0 & 0 & 0 & 0 & 0 & 0 & 0 \\ 0 & 0 & 0 & 0 & f & 0 & 0 & 0 & 0 \\ 0 & 0 & 0 & f^* & 0 & 0 & f^* & 0 & 0 \\ 0 & 0 & 0 & 0 & 0 & 0 & 0 & f^* & 0 \\ 0 & 0 & 0 & 0 & f & 0 & 0 & 0 & 0 \\ 0 & 0 & 0 & 0 & 0 & f & 0 & 0 & f \\ 0 & 0 & 0 & 0 & 0 & 0 & 0 & f^* & 0 \end{pmatrix} \quad \text{(A.11)}$$

$$\boldsymbol{A}_2 = \begin{pmatrix} 0 & 0 & 0 & 0 & 0 & 0 & 0 & 0 & 0 \\ 0 & 0 & 0 & f & 0 & f^* & f & 0 & f^* \\ 0 & 0 & 0 & 0 & 0 & 0 & 0 & 0 & 0 \\ 0 & f^* & 0 & 0 & 0 & 0 & 0 & 0 & 0 \\ 0 & 0 & 0 & 0 & 0 & 0 & 0 & 0 & 0 \\ 0 & f & 0 & 0 & 0 & 0 & 0 & 0 & 0 \\ 0 & f^* & 0 & 0 & 0 & 0 & 0 & 0 & 0 \\ 0 & 0 & 0 & 0 & 0 & 0 & 0 & 0 & 0 \\ 0 & f & 0 & 0 & 0 & 0 & 0 & 0 & 0 \end{pmatrix} \quad \text{(A.12)}$$

$$\boldsymbol{A}_3 = \begin{pmatrix} 0 & 0 & 0 & f & 0 & f^* & 0 & 0 & 0 \\ 0 & 0 & 0 & 0 & 0 & 0 & 0 & 0 & 0 \\ 0 & 0 & 0 & 0 & 0 & 0 & f & 0 & f^* \\ f^* & 0 & 0 & 0 & 0 & 0 & 0 & 0 & 0 \\ 0 & 0 & 0 & 0 & 0 & 0 & 0 & 0 & 0 \\ f & 0 & 0 & 0 & 0 & 0 & 0 & 0 & 0 \\ 0 & 0 & f^* & 0 & 0 & 0 & 0 & 0 & 0 \\ 0 & 0 & 0 & 0 & 0 & 0 & 0 & 0 & 0 \\ 0 & 0 & f & 0 & 0 & 0 & 0 & 0 & 0 \end{pmatrix} \quad \text{(A.13)}$$

$$\boldsymbol{A}_4 = (z(t_j))\boldsymbol{I} + \boldsymbol{A}_{4,\,\mathrm{hyp}} \quad \text{(A.14)}$$

where

$$\boldsymbol{A}_{4,\,\mathrm{hyp}} = \begin{pmatrix} J+h & 0 & 0 & 0 & 0 & 0 & 0 & 0 & 0 \\ 0 & 0 & 0 & 0 & 0 & 0 & 0 & 0 & 0 \\ 0 & 0 & -J-h & 0 & 0 & 0 & 0 & 0 & 0 \\ 0 & 0 & 0 & \frac{J}{2}+\frac{h}{2} & 0 & 0 & 0 & 0 & 0 \\ 0 & 0 & 0 & 0 & 0 & 0 & 0 & 0 & 0 \\ 0 & 0 & 0 & 0 & 0 & \frac{J}{2}+\frac{h}{2} & 0 & 0 & 0 \\ 0 & 0 & 0 & 0 & 0 & 0 & -\frac{J}{2}-\frac{h}{2} & 0 & 0 \\ 0 & 0 & 0 & 0 & 0 & 0 & 0 & 0 & 0 \\ 0 & 0 & 0 & 0 & 0 & 0 & 0 & 0 & -\frac{J}{2}-\frac{h}{2} \end{pmatrix}$$

and J is the time-dependent hyperfine coupling constant

$$j = \frac{1}{2}\left(\frac{g_e \beta_e}{\hbar}\right)(A_{xx} + A_{yy} + A_{zz}). \quad \text{(A.15)}$$

Field tensor components, evaluated in the (L)-frame together with eigenvalues from spin operators given in eqn. (6) and (8) are

$$z(t_j) = B_Z \sqrt{\frac{2}{3}} \sum_{m,k} D^2_{0m}[\Omega_{LD}] D^2_{mk}[\Omega_{DP}(t_j)] F_k^{2(P)g} \quad \text{(A.16)}$$

$$h(t_j) = \sqrt{\frac{2}{3}} \sum_{m,k} D^2_{0m}[\Omega_{LD}] D^2_{mk}[\Omega_{DP}(t_j)] F_k^{2(P)A} \quad \text{(A.17)}$$

$$f(t_j) = -\frac{1}{2} \sum_{m,k} D^2_{-1m}[\Omega_{LD}] D^2_{mk}[\Omega_{DP}(t_j)] F_k^{2(P)A} \quad \text{(A.18)}$$

$$f^*(t_j) = -f(t_j) \quad \text{(A.19)}$$

Tensor components in the principal frame are given in eqn. (2.2). In eqn. (A.19) a symmetry property of ISTO-components is used. The following decomposition due to eqn. (A.5) and (A.6) was made

$$\alpha_1 = 2; \quad \boldsymbol{K}_1(t) = \boldsymbol{A}_1/|f(t_j)| \quad \text{(A.20)}$$

$$\alpha_2 = 4; \quad \boldsymbol{K}_2(t) = \boldsymbol{A}_2/|f(t_j)| \quad \text{(A.21)}$$

$$\alpha_3 = 2; \quad \boldsymbol{K}_3(t) = \boldsymbol{A}_3/|f(t_j)|. \quad \text{(A.22)}$$

Matrix $\boldsymbol{\Lambda}_4(t_j)$ is not expressed using eqn. (A.9) since for a diagonal matrix

$$\exp(\boldsymbol{A}_4(t)) = \mathrm{diag}[\exp(-i\tau A_4(1,1)), \ldots, \exp(-i\tau A_4(9,9))] \quad \text{(A.23)}$$

where the diagonal elements of $\boldsymbol{A}_4(t)$ are given by eqn. (A.14).

References

1 B. H. Robinson, H. Thomann, A. H. Beth, P. Fajer and L. R. Dalton, in *EPR and Advanced EPR Studies of Biological Systems*, ed. L. R. Dalton, CRC Press, Boca Raton, FL, 1985, ch. 5; P. F. Knowles and B. Peake, in *Electron Spin Resonance*, ed. P. B. Ayscough, The Chemical Society, London, 1977, vol. 4, ch. 10.
2 L. Kar, E. Ney-Inger and J. Freed, *Biophys. J*., 1985, **48**, 569.
3 U. Essman and M. L. Berkowitz, *Biophys. J*., 1999, **76**, 2081.
4 S. E. Feller, R. M. Venable and R. W. Pastor, *Langmuir*, 1997, **13**, 6555; H. Loof, S. C. Harvey, J. P. Segrest and R. W. Pastor, *Biochemistry*, 1991, **30**, 2099.
5 D. P. Tieleman and H. J. C. Berendsen, *J. Chem. Phys*., 1996, **105**, 4871.
6 J. W. Essex, M. M. Hann and W. G. Richards, *Philos. Trans. R. Soc. London, Ser. B*, 1994, 239.
7 E. Meirovitch, A. Nayeem and J. H. Freed, *J. Phys. Chem*., 1984, **88**, 3454; R. Kubo, *J. Math. Phys*., 1963, **4**, 174.
8 J. H. Freed, in *Spin Labeling, Theory and Applications*, ed. L. J. Berliner, Academic Press, New York, 1976, p. 53.
9 D. J. Schneider and J. H. Freed, in *Biological Magnetic Resonance, Spin Labeling: Theory and Applications*, ed. L. J. Berliner and J. Reuben, Plenum Press, New York, 1989, vol. 8.
10 M. Moser, D. Marsh, P. Meier, K.-H. Wassmer and G. Kothe, *Biophys. J*., 1989, **55**, 111; A. Lange, D. Marsh, K.-H. Wassmer, P. Meier and G. Kothe, *Biochemistry*, 1985, **24**, 4383.
11 L.-J. Korstanje, E. E. Van Faassen and Y. K. Levine, *Biochim. Biophys. Acta*, 1989, **980**, 225.
12 K. Kinosita, S. Kawato and A. Ikegami, *Biophys. J*., 1977, **20**, 289.
13 C. C. Wang and R. Pecora, *J. Chem. Phys*., 1980, **72**, 5333.
14 Z. Liang and P.-O. Westlund, *J. Chem. Phys*., 1993, **99**, 7090; Z. Liang and P.-O. Westlund, *J. Phys. Chem*., 1984, **88**, 6633; I. Fedchenia, P.-O. Westland and U. Cegrell, *Mol. Simul*., 1993, **11**, 373.
15 E. Lindahl and O. Edholm, *J. Chem. Phys*., 2001, **115**, 4938.
16 M. S. Itzkowitz, *J. Chem. Phys*., 1967, **46**, 3048.
17 J. B. Pedersen, *J. Chem. Phys*., 1972, **57**, 2650.
18 B. H. Robinson, L. J. Slutseg and F. P. Auleri, *J. Chem. Phys*., 1992, **90**, 2609.
19 A. Ferrarini, P. L. Nordio, G. J. Moro, R. H. Crepeau and J. H. Freed, *J. Chem. Phys*., 1989, **91**, 5707; A. Ferrarini, P. L. Nordio, G. J. Moro, R. H. Crepeau and J. H. Freed, *J. Phys. Chem*., 1971, **75**, 3385; A. Ferrarini, P. L. Nordio, G. J. Moro, R. H. Crepeau and J. H. Freed, *J. Chem. Phys*., 1971, **55**, 5270; D. J. Schnider and J. H. Freed, *Adv. Chem. Phys*., 1989, **73**, 387.
20 N. Usova, P.-O. Westlund and I. Fedchenia, *J. Chem. Phys*., 1995, **103**, 96.
21 N. Usova, L. Persson and P.-O. Westlund, *Phys. Chem. Chem. Phys*., 2000, **2**, 2785.
22 D. M. Brink and G. R. Satchler, *Angular Momentum*, Clarendon Press, Oxford, 3rd edn., 1993.
23 E. Egberts, S. J. Marrink and H. J. C. Berendsen, *Eur. Biophys. J*., 1994, **22**, 423.
24 O. Berger, O. Edholm and F. Jähnig, *Biophys. J*., 1997, **72**, 2002.
25 E. Lindahl and O. Edholm, *Biophys. J*., 2000, **79**, 426.
26 E. Lindahl and O. Edholm, *J. Chem. Phys*., 2000, **113**, 3882.
27 H. J. C. Berendsen, J. P. M. Postma, A. DiNola and J. R. Haak, *J. Comput. Phys*., 1984, **81**, 3684.
28 H. J. Berendsen, D. van der Spoel and R. van Drunen, *Comput. Phys. Commun*., 1995, **91**, 43.
29 B. Hess, H. Bekker, H. J. C. Berendsen and J. G. E. M. Fraaije, *J. Comput. Chem*., 1997, **18**, 1463.
30 J. P. Ryckaert, G. Ciccotti and H. J. C. Berendsen, *J. Comput. Phys*., 1977, **23**, 327.
31 J. F. Nagle and M. C. Wiener, *Biochim. Biophys. Acta*, 1988, **942**, 1.
32 J. F. Nagle, R. T. Zhang, S. Tristram Nagle, W. J. Sun, H. I. Petrache and R. M. Suter, *Biophys. J*., 1996, **70**, 1419.
33 O. Edholm and C. Blomberg, *Chem. Phys*., 1999, **252**, 221.
34 C. P. Slichter, *Principles of Magnetic Resonance*, Springer-Verlag, Berlin, 1990.
35 H.-J. Steinhoff and W. L. Hubell, *Biophys. J*., 1996, **71**, 2201.